Set-Up for Nuclear Reaction studies at Ion StoragE rings (SUNRISE)

1. *Motivation and state of the art*

The synthesis of elements from iron to uranium takes place in stars. It has been established that most of these elements are produced during the slow (*s*) and rapid (*r*) neutron-capture processes [Bur57]. The mentioned processes are distinguished by the neutron density in the astrophysical scenario. If the neutron density is low, unstable nuclei will decay more likely than capture a neutron (s-process). However, if the neutron density is very high, seed nuclei will capture many neutrons in a row and form very heavy isotopes before they decay (r-process). Therefore, the **synthesis of elements** can only be understood through **the knowledge of neutron-induced reaction cross sections of radioactive nuclei** [Rei14], which are often **very difficult or even impossible to measure**.

A neutron-induced reaction can be described as a two-step process (Fig. 1). In the first step the nucleus *A* will absorb the neutron forming a compound nucleus (*A*+1)*. A compound nucleus (CN) is a nucleus in statistical equilibrium. The excited CN can then decay in different ways, by emitting γ-rays, by emitting a neutron or, if the CN is heavy enough, it can fission, i.e. split into two lighter nuclei.

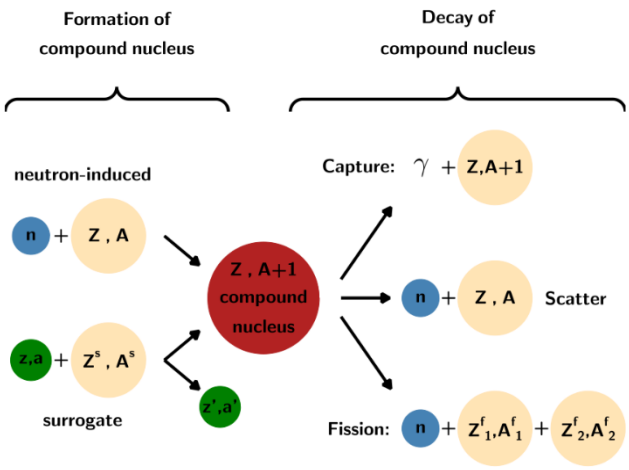

Figure 1: *Description of a neutron-induced reaction. The de-excitation channels of the compound nucleus via γ-emission (radiative capture), neutron emission (scattering) and fission are shown. In a surrogate reaction, the compound nucleus is produced by a different reaction.*

Since most of the seed nuclei are radioactive, most of the neutron-induced cross sections of astrophysical interest rely on **theoretical model predictions that are subject to significant uncertainties**. Regarding the s-process, further progress is stalled due to the lack of good-quality neutron cross sections, hampering the models to constrain fundamental assumptions about the hydrodynamics in stars or the age of the Universe [Pig10]. As for the r-process, even if neutron star mergers are a strong candidate to host the process [Kas17], there are still huge uncertainties related to nuclear reaction data with predictions for the neutron cross sections that often disagree by several orders of magnitude [Mum16, Thi17]. **Neutron-induced radiative capture cross sections** are among the **most uncertain of the nuclear data inputs** for the r-process. Sensitivity studies described in [Mum16] show that the key nuclei are concentrated near closed shells and in the rare-earth region, where they impact the formation of the rare-earth peak of the r-process abundance pattern. **Spontaneous and neutron-induced fission** of very neutron-rich heavy nuclei **play also an essential role during r-process nucleosynthesis in neutron-star mergers**, as they determine the end of the r-process path and the fission products strongly influence the nuclide abundances [Gor15]. According to [Gor15, Eic15] the nuclei that play a major role are located near the N=184 shell closure with Z≈90-98.

Neutron cross sections of short-lived nuclei are also important for industrial purposes, e.g. for energy production and for the search of novel therapeutic radionuclides for diagnostic and treatment.

Direct measurements of neutron cross sections on unstable isotopes are **very difficult**: (a) The radiative capture measurements need to detect the γ-rays in the presence of a γ-ray background following the decay of the sample material. (b) The neutron scattering measurements need to distinguish the neutrons scattered by the nucleus of interest from the huge background of neutrons scattered by the surrounding materials. (c) The fission measurements face the background from α-

emission or spontaneous fission competing with the signals from the neutron-induced fission. (d) The radiation from the radioactive sample can severely damage the detectors. (e) The production and handling of radioactive samples is severely restrained by health and safety regulations.

In the case of **charged-particle-induced reactions**, **the challenges of radioactive samples are often solved by inverting the kinematics of the reaction**. This means accelerating the heavy nucleus while keeping at rest the light particles (protons, deuterons, α-particles…), which act as a target. There are several radioactive-ion-beam (RIB) facilities world-wide following this approach. However, the inversed-kinematics technique is **not possible for neutron-induced reactions**, since free neutron targets are unavailable at least for the next two decades [Rei17].

1.1. Surrogate reactions

The **most promising approach** to overcome the difficulties associated with the measurement of neutron cross sections of radioactive nuclei is to use **surrogate reactions in inverse kinematics**. The surrogate reaction produces the compound nucleus of interest by a different reaction than the neutron-induced reaction (compare Fig. 1) and the decay probabilities for γ-emission, neutron emission and fission are measured. The measured decay probabilities of the compound nucleus are used to constrain model parameters (fission barriers, particle transmission coefficients, level densities, etc.) and enable much more accurate predictions of the desired neutron cross sections. Of particular interest is the so-called **(d,p) reaction**, which stands for (^{2}H,^{1}H). In the experiment, a heavy-ion beam is directed onto a deuterium gas target. During the particle exchange, the neutron of the deuterium target is passed on to the projectile nucleus. Therefore, the (d,p) reaction appears intuitively as the **closest reaction to a neutron-induced reaction in inverse kinematics**.

An interesting aspect of surrogate reactions is that several reactions can be investigated simultaneously with a single projectile-target combination. For instance, in an experiment involving a heavy projectile *A* and a D_2 deuterium target, it will also be possible to investigate the inelastic-scattering reaction of deuterons -denoted (d,d')- where the deuteron is scattered leaving the heavy projectile *A* in an excited state *A**. One can also study the (d,t) reaction, where the target nucleus removes a neutron from the projectile forming the excited nucleus (*A*-1)*. An additional advantage of surrogate reactions is that with one incident beam energy it is possible to populate a broad excitation-energy distribution of the heavy residue (from 0 to about 15 MeV) and measure the decay probabilities of the different nuclei as a function of excitation energy. To infer the decay probabilities in inverse kinematics it is necessary to identify the different target-like residues, precisely measure their energy and emission angle with respect to the beam to calculate the excitation energy of the CN, and detect the products of the CN decay in coincidence with the target-like residues.

Fission probabilities induced by nuclear transfer and inelastic-scattering reactions represent the most direct observable to infer fission barriers and are also a unique tool to study the level structure and the level density in the vicinity of the fission barrier [Kes15]. Note that fission barriers have a dramatic impact on spontaneous fission half-lives, a modification of the fission barrier of typically 1 MeV can affect the half-live up to 9 orders of magnitude. A particularly interesting aspect of **fission probabilities** is that they **can be used to infer neutron-induced fission cross sections by applying the "Weisskopf-Ewing" (WE) approximation.** Within the WE approximation, the decay of a CN is considered to be independent of its spin and parity; i.e., it is assumed that the decay probabilities of the CN are identical for the neutron-induced and the surrogate reactions [Esc12]. In this case, the desired neutron cross section can be obtained applying the equation:

$$\sigma_{n,\chi}(E_n) = \sigma_n^{CN}(E_n) \cdot P_{s,\chi}(E^*) \quad (1)$$

where $\sigma_n^{CN}(E_n)$ is the cross section for the formation of a CN after the absorption of a neutron of incident energy E_n, E^* is the excitation energy of the CN and $P_{s,\chi}$ is the probability that the CN formed by the surrogate reaction decays via channel χ. The CN formation cross section σ_n^{CN} is calculated with optical potentials and has an uncertainty of less than 10% for nuclei not very far from stability

[Esc12]. The factorization of the cross section in eq. (1) into the product of the formation cross section and the decay probability reflects the independence of the formation and the decay steps inherent to the formation of a CN.

A number of examples involving actinides not far from ^{238}U measured in direct kinematics by the CENBG collaboration [Pet04, Kes10, Jur17] and by other groups in the USA [Esc12] show that the fission cross sections derived using eq. (1) are in very good agreement with directly measured neutron-induced fission cross sections. This is particularly useful since the theoretical predictions for the fission probabilities are quite uncertain because of the lack of knowledge on the level structure in the vicinity of the fission barrier. In addition, to infer the fission probabilities one has also to model the competition with all the other open decay channels. This requires an accurate knowledge of the nuclear structure properties of the nuclei involved in the decay, which is available to some extent only near the stability valley where experimental data exist.

However, the Lawrence Livermore National Laboratory in the USA [Sci10] and the CENBG [Bou12] collaborations observed that **the radiative-capture cross sections of rare-earth nuclei obtained with eq. (1) were up to a factor 10 larger than the directly measured neutron-induced cross sections.** These significant differences have been attributed to the higher angular momenta populated in the surrogate reaction. Indeed, at excitation energies close to the neutron separation energy S_n, neutron emission is very sensitive to the angular momentum of the decaying nucleus A^*, because only the ground state and the first excited states of the residual nucleus (A-1) formed after neutron emission can be populated. When the angular momentum of A^* is much larger than the angular momentum of the first states of nucleus (A-1), neutron emission is hindered and the excited nucleus A^* predominantly decays by γ emission, which is the only open decay channel [Bou12].

It is surprising that the spin/parity mismatch between surrogate and neutron-induced reactions has no major impact on the measured fission probabilities, not even at energies around the fission threshold. Indeed, the energy region close to the fission barrier is also characterized by a low density of states and a significant dependence of the fission probability on the angular momentum is expected by theory [Esc12]. To shed light into this puzzling observation, the CENBG collaboration has carried out a campaign of experiments in direct kinematics to measure for the first time simultaneously fission and γ-decay probabilities for various excited nuclei with different structural properties. We have considered nuclei with an odd number of protons and/or neutrons, such as ^{238}Np or ^{237}U, and nuclei with an even number of protons and neutrons like ^{240}Pu. The level density above the fission barrier for even-even nuclei is significantly lower than for nuclei with an odd number of protons or neutrons, and a stronger sensibility to angular momentum differences is expected. We have observed that for ^{238}Np and ^{237}U, the fission cross sections obtained applying the WE approximation are in very good agreement with the neutron-induced data, whereas there are large discrepancies between the radiative capture cross sections [Jur17]. However, in the case of the even-even ^{240}Pu nucleus there are significant discrepancies between the neutron cross sections and the ones obtained with eq. (1) for both, the fission and the radiative capture cross sections [Per19a].

When the WE approximation fails, a different strategy is needed. This strategy consists in **predicting the spin and parity distributions** populated in the surrogate reaction and **using the decay probabilities induced by the surrogate reaction to fix the values of the parameters** of some of the key ingredients of the statistical model like fission barriers, neutron transmission coefficients, level densities and γ-ray strength functions. With the newly-tuned parameters the model gives an **accurate prediction of the desired neutron cross section**. This strategy has recently been proven for radiative neutron capture in two benchmark experiments where the emission probabilities for selected γ-ray transitions were measured. In [Esc18], the ^{92}Zr(p,d) reaction was used to infer the well-known ^{90}Zr(n,γ) cross section, and in [Rat19] the ^{95}Mo(d,p) reaction was used to infer the ^{95}Mo(n,γ) cross section. As shown in [Rat19], the use of the **(d,p) reaction** requires also modeling the **complex deuteron breakup process** where the transferred neutron escapes before the formation of the CN.

The results of applying this alternative strategy far from stability will be significantly improved if all the decay probabilities are measured simultaneously, because these data will constrain the model parameters for all the open decay channels. Note that measuring the decay probabilities for all the open decay channels provides also a **strong test to the experimental technique**, because the sum of the probabilities must be equal to 1 [Jur17]. Besides, it will also be very useful to **measure simultaneously the angular distributions of the target-like reaction products**, since they will strongly **constrain the models used to predict the spin-parity distribution** of the surrogate reaction.

To establish whether the methods based on surrogate reactions described above can be used to infer neutron-induced cross sections in regions where no neutron data exist, it is **necessary to build the systematics of decay probabilities over isotopic chains involving nuclei in various mass regions**. For heavy nuclei, surrogate reactions have only been investigated in a limited region of well-deformed neutron-rich actinides close to ^{238}U. Therefore, it would be for example highly interesting to investigate nuclei located around the ***N*=126 shell closure**. Beams of these nuclei are available at the GSI/FAIR facility in Darmstadt, Germany. These studies will help to provide much **better predictions for the cross sections near the shell closure *N*=184**, which is not yet accessible to experiments. Since the populated spin-parity distribution depends on the nuclear reaction used, **one can investigate the influence of the spin and parity by comparing the probabilities obtained with different surrogate reactions that lead to the same excited nucleus**. By doing this we can verify whether the values deduced for the model parameters depend on the surrogate reaction used. Spin-parity effects can also be investigated by **comparing the decay probabilities measured at different emission angles** of the target-like reaction residues, because the populated spin-parity distribution depends on this angle too[Esc12].

These systematic studies cannot be performed with standard techniques. Indeed, the measurement of **surrogate reactions in direct kinematics faces the following limitations**: (a) Unavailability of targets from short-lived nuclei. (b) High background from the competing reactions with the target contaminants and backing. (c) The heavy products of the decay of the CN are stopped in the target and cannot be detected with particle detectors. Therefore, the measurement of γ- and neutron-emission probabilities in direct kinematics relies in the detection of the γ-rays or the neutrons emitted by the compound nucleus, which is very difficult due to the very low detection efficiencies. **The limitations (a) and (c) can be addressed with the inverse kinematics technique**.

Experiments in inverse kinematics with radioactive ion beams require a high areal density of target atoms. However, the different isotopes of H, as the most promising candidates for surrogate reactions, are gases. **This creates many difficulties**: (1) Pressurized gas cells require entrance and exit windows. The beam can interact with the window generating a strong background. (2) Chemical compounds like CH_2 have the same disadvantages as windows. (3) Windowless gas targets with high areal densities are large. This results in a very limited resolution of the interaction point. (4) The resolution of the emission angle relative to the direction of the incoming particles is reduced if the beam straggles in the target material before the reaction. (5) The ions lose energy by interacting with the electrons of the thick gas target. The center-of-mass energy of the reaction is therefore uncertain and limits the knowledge of the excitation energy of the compound nucleus. The experiments described so far are called single-pass experiments, because each ion passes the target only once. Afterwards the expensively produced ion is lost.

1.2. Heavy-ion storage rings

Heavy-ion storage rings offer **unique and largely unexplored opportunities** to investigate surrogate reactions in inverse kinematics. Presently, there are only two heavy-ion storage rings in full operation worldwide: the Experimental Storage Ring (ESR) [Fra87] at GSI/FAIR and the Cooler-Storage Ring (CSRe) [Xia02] at the Institute of Modern Physics in Lanzhou. Two other rings, the CRYRING [Les16] at GSI/FAIR and the Rare-RI ring at Riken [Yam13] have just entered in the operation phase. A storage ring for nuclear-physics experiments at HIE-ISOLDE, CERN, is currently being designed [Gri19].

A storage ring is a type of circular lattice of bending and focusing magnetic multipoles (dipoles, quadrupoles, etc.) whose purpose is to accumulate and store radioactive ions up to the highest possible currents. The stored ions turn with high frequencies, about 1 MHz at 10 A MeV. The storage of heavy ions needs to ensure a minimum of atomic reactions between the stored beam and the residual gas inside the ring. Therefore, heavy-ion storage beams are operated in ultra-high vacuum (UHV) conditions (10^{-10} to 10^{-12} mbar). The most important capability of storage rings is beam cooling, which allows for a significant reduction of the energy and position spread of the stored ions induced by the reaction mechanism used to produce them or by the interaction with internal targets. Beam cooling takes typically a few seconds, which sets the lower limit of the half-live of the radioactive ions that can be prepared. The combination of the electron cooler and the dipole magnets ensures an **extraordinary quality of the stored beam in terms of emittance and purity**. If a gas target is present, the electron cooler can compensate the energy loss and the straggling of the beam in the gas target. Hence, the ions pass the target always with the same energy and the same momentum spread –quite in contrast to most single-pass experiments. Moreover, **the frequent passing of the reaction zone allows ultra-thin gas targets** (10^{13} atoms/cm^2) to be used and **no windows** are necessary. This is of great advantage for surrogate reactions since the beam will only interact with the desired material and in a **well-defined interaction zone**. Furthermore, the **outstanding beam quality, along with the negligible straggling enables a precise measurement of the excitation energy of the decaying nucleus. All these advantages are only possible with storage rings.**

Storage rings can be used as synchrotrons to accelerate or decelerate stored beams to the required energy. Stored highly-charged radionuclides can presently be slowed down at the ESR only. The available beam energies at the ESR are from about 400 A MeV, typical injection energy, down to about 4 A MeV. Secondary beams produced in-flight via fragmentation reactions or fission can be separated with the Fragment Separator and injected into the ESR. The production of fully stripped heavy ions requires energies of typically 100 A MeV. Therefore, the deceleration capabilities of the ESR are particularly interesting, since they allow the **production of 10 A MeV cooled beams with fully stripped heavy ions.** In addition, owing to the high resolving power achievable with electron-cooled beams, the ESR can prepare **mono-isotopic beams**.

GSI/FAIR is the only facility worldwide where two heavy-ion storage rings are connected together (CRYRING@ESR). The ESR is used to slow down and cool the beams that are then injected into the CRYRING, which is optimized for the storage of ions at low energies, from 14.5 A MeV down to few tens of A keV for $^{238}U^{92+}$. The combination of the CRYRING with the ESR is particularly interesting since the CRYRING is used to perform the measurements with the cooled ions, while the ESR prepares the next ion bunch. In this way, **no time is lost in the preparation of the beam**. Because of the low beam energies, the vacuum conditions at the CRYRING have to be even better than at the ESR, 10^{-11}-10^{-12} mbar.

The UHV environment poses severe constraints to in-ring detection systems because the vacuum conditions have to be improved by 6-7 orders of magnitude compared to single-pass experiments. For this reason nuclear reactions have started to be measured only very recently at the ESR. The possibility to measure proton-induced radiative-capture cross sections in the ESR was first demonstrated with the successful measurement of the ^{96}Ru(p,γ) cross section at 10 A MeV [Mei15]. Very recently, the ^{124}Xe(p,γ) cross section was measured at even lower energies of only 5.5 A MeV [Glo19]. **These pioneering experiments have been proposed and lead by a collaboration between the University of Frankfurt and the GSI**.

2. Objectives

The objectives of this proposal are to **develop a setup and a methodology** to **simultaneously** measure **fission, γ and particle-emission probabilities induced by transfer or inelastic-scattering reactions in inverse kinematics** at the **CRYRING storage ring**, and to conduct a **first experiment** with a **^{238}U beam** at 11 A MeV on a **deuterium gas-jet target**.

The kinematics of two-body reactions involving a heavy projectile (^{238}U) at 11 A MeV and a light target (^{2}H) leads to target-like residues covering a broad range of angles from 0 to 180°, whereas the associated projectile-like residues are very much forward focused with maximum emission angles of less than 0.5°. The fission fragments are emitted within a cone of about 20°. The **required set-up** is presented in Fig. 2. It consists of: (a) a **particle telescope** Δ*E*-*E* to identify and measure the kinetic energies and angles of the target-like nuclei. (b) A **fission detector** covering angles in forward direction to detect fission fragments in coincidence with the target-like detectors. (c) A **detector for** counting the number of **heavy beam-like products** formed after γ-ray or neutron emission measured in coincidence with the target-like detectors. The latter detector is placed after the second dipole downstream from the reaction zone. The dipoles will separate the beam and the different beam-like residues according to their magnetic rigidity.

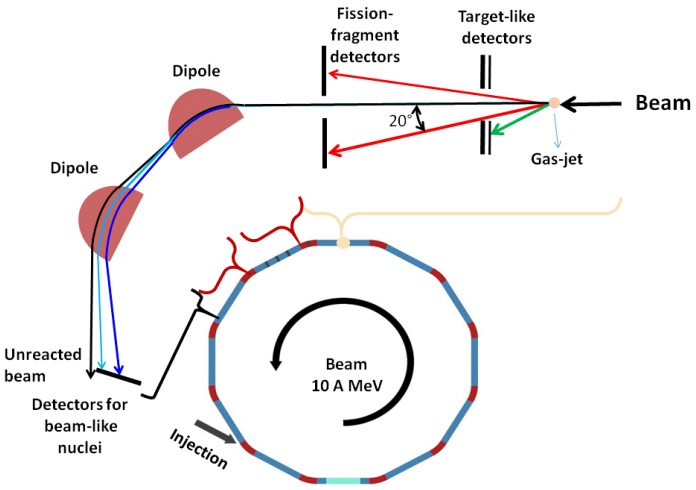

Figure 2: *The upper part shows a schematic view of the experimental setup that will be placed inside the CRYRING for the simultaneous measurement of fission, γ- and particle-emission probabilities. The trajectories of the beam-like residues produced after γ and neutron emission are shown in light blue and blue, respectively. They are detected after the second dipole downstream from the target. The CRYRING storage ring is shown in the lower part.*

The decay probabilities are given by:

$$P_{s,\chi}(E^*) = \frac{N_{c,\chi}(E^*)}{N_t(E^*)\cdot\varepsilon_\chi(E^*)} \qquad (2)$$

where N_t is the number of target-like nuclei detected, $N_{c,\chi}$ is the number of coincidences measured between the residues of decay channel χ and the target-like nuclei, and ε_χ is the efficiency for detecting the residues of decay channel χ.

As in the proton-capture experiments [Mei15, Glo19], our set-up will be completed with **high-purity germanium detectors** surrounding the target (not shown in Fig. 2). They will be used to detect the x-ray signature of the radiative electron (e^-) capture process. The cross sections for this process can be predicted with an uncertainty ≤ 2% and are very well suited **for determining the luminosity** in the ring. With this information, it will be possible to **determine the cross sections as a function of angle** of the target-like nuclei, which are very useful for predicting the populated spin-parity distributions.

2.1. Detection system for target-like residues

The interaction of ^{238}U at 11 A MeV with a D_2 target leads to the simultaneous population of various two-body reactions, mainly ^{238}U(d,p), ^{238}U(d,d') and ^{238}U(d,t). Therefore, a particle telescope is necessary to distinguish between the different target-like residues. As shown in Fig. 1, the telescope will be placed at forward angles downstream from the gas-jet target. It will be constituted by two detectors located inside retractable pockets. The two pockets will be inserted in a reaction chamber that surrounds the gas-jet target. The detectors will be separated from the UHV of the reaction chamber by a stainless steel window of 25 μm. Pockets with such type of windows are very often used at the ESR. One of them was used in the first ESR proton-capture experiment [Mei15]. Each pocket will contain a thin, 1 mm-thick, position-sensitive Δ*E* detector for measuring the angle and the energy-loss, followed by a 12 mm-thick *E* detector made of a stack of two Si(Li) detectors, which stops the target-like residues. The distance between the pocket window and the Δ*E* detector will be 4 mm.

For reactions in inverse kinematics involving a heavy projectile and a light target, a very strong correlation between the energy of the target-like nuclei and the emission angle has to be taken into

account. A very high angular resolution ($\Delta\theta \approx 0.1°$) is thus necessary to obtain an excitation-energy resolution of few hundred keV. Therefore, the ΔE detector will be a **highly segmented double-sided silicon strip detector (DSSSD)** with 128x48 channels and 128x48 mm^2 size. For the E detectors we will use four large-area, 6 mm-**thick Si(Li) detectors**. The auxiliary vacuum in the pocket will be 10^{-6}-10^{-7} mbar. One of the pockets will be placed 2 cm above the beam and the other 2 cm below, leaving a gap in the center to enable the undisturbed passage of the unreacted beam, beam-like residues and the fission fragments, see Fig. 1. The two pockets are placed at 4 cm from the target. Highly segmented DSSSDs can be purchased from the company Micron Semiconductors [Micro] and large-area Si(Li) detectors of 6 mm thickness are currently manufactured for example by Canberra [Canbe]. The main characteristics of the detectors for the target-like residues are resumed in Table 1.

Detector	Detector type and quantity	Size	Number of channels	Angular coverage
Telescope ΔE	2xDSSSD (1 mm thick)	128x48 mm^2	2x(128+48)	25 to 66°
Telescope E	8xSi(Li) (2x6 mm thick)	≈65x55 mm^2	8	25 to 66°

Table 1: *Main characteristics of the detectors for target-like residues.*

We have performed very **detailed Geant4 simulations** for the inelastic scattering ^{238}U(d,d') reaction, where we have tracked all the reaction residues from the target until the different detectors. Fig. 3 shows the simulated excitation-energy distribution associated to deuteron residues emitted at 40° and corresponding to an excitation energy of the beamlike ^{238}U* residue of 8.2 MeV. This excitation energy is about 2 MeV above the neutron separation energy of ^{238}U, which amounts to 6.1 MeV. Thanks to the electron cooling it is possible to neglect the straggling of the ^{238}U beam in the D_2 target, but we have considered the straggling of the scattered deuterons in the stainless-steel window of the pocket. The effect of the latter on the excitation-energy resolution is negligible.

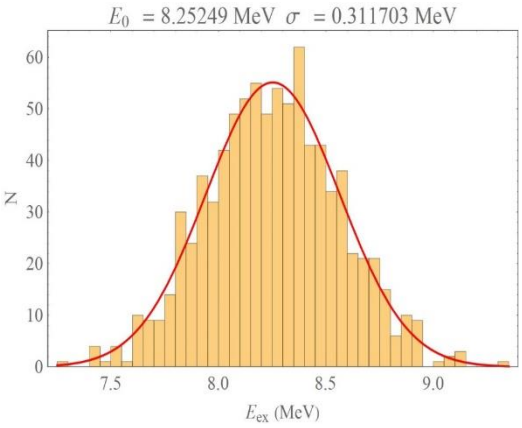

Figure 3: *Simulated excitation energy distribution for the ^{238}U(d,d') reaction. The standard deviation σ is indicated.*

In addition, we have considered the detector segmentation, the diameter of the gas-jet target of 0.5 mm, a beam momentum resolution $\sigma P/P = 2 \cdot 10^{-4}$, a beam emittance of 0.05 mm·mrad and an energy resolution of the telescope of $\sigma E/E = 2\%$. As shown in Fig. 3, our simulations give an **excitation-energy resolution $\sigma E^* \approx 300$ keV**. This value is mainly determined by the energy resolution of the telescope. If the beam emittance is increased to 0.5 mm·mrad or the detector resolution to 6%, we obtain $\sigma E^* \approx 500$ keV. These values σE^* are **adequate to study the rapid variation of the decay probabilities** at the fission and particle threshold, and are **comparable to** what is typically obtained in **direct-kinematics**.

2.2. Detection system for fission fragments

Solar cells, the devices that are routinely used to convert the energy of sunlight into electricity, represent a **particularly interesting option for the detection of fission fragments inside a storage ring**. **The CENBG has many years of experience** using them as fission detectors [Pet04, Kes10, Per19b]. Solar cells offer many advantages compared to other detector concepts: First, they are solid-state detectors, which are much simpler to use in UHV than gaseous detectors. Second, the resolution of the energy carried by fission fragments with about 1 A MeV is nearly 2%, which is comparable to what can be obtained with Si detectors [Sie79, Aji91, Gau97]. Third, solar cells are much more resistant to radiation damage than Si detectors [Aji91, Gau97]. This radiation hardness is of significant advantage for in-ring measurements, since replacing damaged detectors implies venting the reaction chamber. Re-establishing UHV, even in a small portion of the ring, typically takes a few days.

The thickness of solar cells varies between 300-500 μm but their depletion depth is less than 1 μm, hence very small, and it cannot be increased by applying a bias voltage because this increases the electronic noise, due to their very low resistivity of a few Ω·cm. The very small depletion depth leads to a **very large capacitance**, of the order of 40 nF/cm^2. To obtain good timing performances with such a high capacitance **we will use specially designed**, current-mode **preamplifiers designed at the CENBG.** Because of the very thin depletion depth, most of the energy deposition occurs in the neutral substrate. The charge collection in the cell is possible thanks to the "funneling" mechanism [Hsi81], where the high density of ionization produced along the heavy-ion track locally changes the depletion region into a funnel-like shape extending to the substrate and enclosing the track. This enables the collection of a significant part of the charge produced by the fission fragments via ionization. The funneling efficiency strongly depends on the ionization density profile and is very small for light particles. Therefore, the signals induced by the fission fragments will be easy to distinguish from those induced by the elastic scattered deuterons. Solar cells are very robust and can be cut into various shapes (strips, annular detectors) without showing any deterioration. Last but not least, they are extremely cost-effective and well-adapted to build detectors covering large surfaces.

Detector	Detector type and amount	Size	Angular coverage	Fission detection efficiency
Fission	225 Solar cells (~300 μm thick,1x1 cm^2)	4x15x15 cm^2	2 to 33°	80%

Table 2: Main characteristics of the fission detection system, which is placed at 35 cm from the target.

Simulations with fission events generated with the GEF code [Sch16] show that the forward focusing of the fission fragments in inverse kinematics results in a **detection efficiency** for fission fragments **as high as 80%** using a detector made of four smaller detectors with an area of 15x15 cm^2 each, placed at 35 cm from the target. In this case, the required central gap is only of 2 cm^2, see Fig. 2. Because of the very high efficiency, the impact of the fission-fragment angular anisotropy on the efficiency is negligible. Therefore, in contrast to experiments in direct kinematics where the fission efficiency is typically 50%, it is not necessary to measure the angular distribution of the fission fragments, and only a moderate segmentation (15 x15 strips) is required. The solar cells will be mounted on pockets. In this case, the pocket cannot have a stainless-steel window since the less energetic fission fragments, with energies of only a few A MeV, would be stopped. Therefore, **the cells will serve as an active window** separating the UHV of the storage ring from the auxiliary vacuum in the pocket, which accommodates the non-bakeable parts of the system like the cables and electronics. The cells will be mounted on ceramic boards, a material which is non-out gassing and bakeable. DSSSDs have already been used as active windows at the ESR [Str11]. During the ^{124}Xe(p,γ) experiment [Glo19], **it was possible to operate in UHV a** 16x16 channel **DSSSD with cables**. The main characteristics of the fission detector are listed in Table 2.

To use solar cells in our measurements, it is first necessary to determine the efficiency of the charge collection for fission fragments at energies above 1 A MeV and to check their UHV compatibility. To our knowledge, these two aspects have never been investigated before. In 2018, we investigated the energy and time response of solar cells to ^{84}Kr and ^{129}Xe beams with energies ranging from 2 to 15 A MeV at the GANIL facility in Caen, France. We tested cells of different sizes and different substrate material with already-available preamplifiers. We obtained an energy resolution σE/E =2-3% and a time resolution of 4 ns (FWHM). We observed that the quality of the response of the cells started to be deteriorated at rates well above 10 kHz. The highest fission rates in our experiments will come from fusion-fission reactions and will amount to few 100 Hz. Note that these events can be easily removed by the coincidence selection because they are not accompanied by a light target-like nucleus. The very good performances observed during the GANIL tests **validate the use of solar cells for counting fission fragments with energies above 1 A MeV in coincidence** with target-like nuclei**.** We expect that the performances can be even better with the **optimized pre-amplifiers** that **will be developed by the CENBG**. Further tests with optimized electronics are foreseen in 2019 at GANIL and GSI.

The **UHV compatibility** of solar cells has started to be investigated at GSI and at the vacuum test bench of the CENBG. **The first results are very promising** since the outgasing rates are below $5x10^{-11}$ mbar·l/(s·cm^2). We would like to stress that the success of **these studies on solar cells** can have implications that **go well beyond the use of solar cells at storage rings, they can significantly improve the detection and diagnostic methods used in the RIB facilities all around the world.**

2.3. Detection system for beam-like residues

In direct kinematics, it is not possible to detect the heavy residues of the reaction and the γ-emission probability is measured by counting γ rays with detection efficiencies varying from 5 to 10% [Bou12, Duc16, Jur17, Per19b]. Because of the difficulty to detect neutrons, the neutron-emission probability is generally not measured. The situation is radically different in inverse kinematics where the detection of heavy residues is possible. To determine the γ- and neutron-emission probabilities (see eq. 2) we have to be able to discriminate between the beam-like residues *A* and *A*-1 produced after prompt-γ and prompt-neutron emission, respectively, and to evaluate the detection loses in order to infer the associated detection efficiencies. The two residues will go through the different magnetic elements and will be deflected by the two dipoles located downstream from the gas-jet target, see Fig. 2. Because of its smaller mass, the residue *A-1* will be more strongly bent by the dipoles to the inner part of the ring, following a different trajectory than residue *A*. The best discrimination between the two residues is achieved at the focal point of CRYRING, which is located at the end of the straight section placed after the second dipole, see Fig. 2.

We have used our Geant4 simulations to evaluate the discrimination between the residues produced after prompt γ and neutron emission. Again, we have considered the events produced in the ^{238}U(d,d') reaction at 11 A MeV corresponding to an excitation energy of ^{238}U* of 8.2 MeV and where the scattered deuteron is emitted at 40°. Fig. 4 shows the position of the residues at the focal point. The simulation includes the recoil experienced by the ^{237}U nucleus after neutron emission, which broadens the position distribution. This broadening has been included in the most conservative way, i.e. by assuming that the nucleus ^{237}U is in the ground state after neutron emission and therefore, the neutron carries the largest possible kinetic energy.

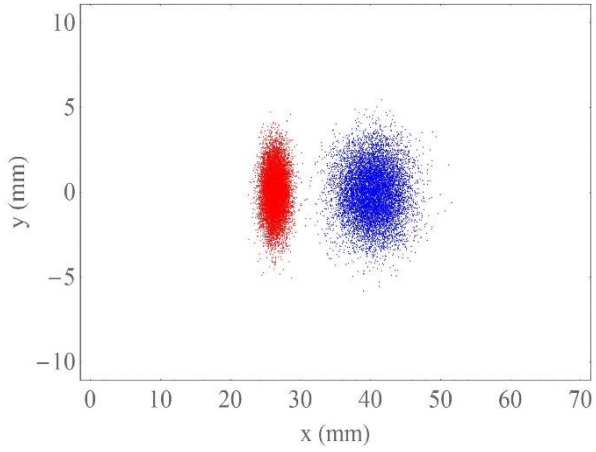

Figure 4: *Position of the residues formed after γ, ^{238}U(red), and neutron emission, ^{237}U(blue), at the focal point for the ^{238}U(d,d') reaction.*

Fig. 4 shows that **the position distributions of the two residues are very well separated from the beam nuclei** (which are at x=0) **and also from each other.** The detector will be positioned at x > 10 mm to let the beam and the elastic scattered ^{238}U residues pass through. Indeed, most of the elastic scattered ^{238}U nuclei are emitted with nearly zero degrees and have almost the same energy as the beam. Therefore, their position at the focal point will be very close to the beam position, x=0. **One DSSSD with 16x16 strips** should be sufficient to achieve the required position resolution. Table 3 shows the characteristics of the beam-like residue detector. The detector will be placed in a **windowless**, retractable **pocket similar to the ones used** for the ^{124}Xe(p,γ) measurement, which will in turn be located in a reaction chamber.

Detector	Detector type	Size	Number of channels	Detection efficiency
Heavy residue	DSSSD (~500 µm)	50x50 mm^2	(16+16)	97-100%

Table 3: Main characteristics of the detector for beam-like residues.

We have also considered the transmission of the residues through the beam lines, dipoles and quadrupoles down to the focal point. We obtain that 100% of the beam-like ^{238}U residues and 97% of the ^{237}U residues reach the focal point. This implies **detection efficiencies** for inferring γ and neutron-emission probabilities **close to 100%**, **much larger than** the efficiencies obtained **in direct kinematics**.

Notice that **we will not have to deal with the intense background** coming from ^{238}U residues **produced after e$^-$ stripping** reactions in the D_2 target, since the ^{238}U stored ions are fully stripped. The **^{238}U residues** produced **after e$^-$ capture in the target are not an issue neither** because they have a smaller charge, i.e. a larger magnetic rigidity, and are bent outside the ring, in opposite direction to the ^{238}U (γ) and ^{237}U (neutron-emission) residues.

2.4. Experiment

The ultimate goal of SUNRISE is to perform a first experiment with the newly developed detection system to investigate surrogate reactions induced by a ^{238}U beam on a D_2 target. With this target-projectile combination it will be possible to **measure simultaneously all the decay probabilities as a function of excitation energy of three reactions ^{238}U(d,t), ^{238}U(d,d') and ^{238}U(d,p)**. The two first reactions will be very useful to **validate the technique**, since the measured decay probabilities P_i have to fulfill that $\sum_i P_i = 1$. For example, at E* below the fission and neutron thresholds the only open decay channel is γ-emission. Thus, P_γ=1, and, according to eq. (2), $\varepsilon_\gamma = N_{c,\gamma}/N_t$. Therefore, the simulated efficiency for detecting the residues formed after γ emission has to be equal to the ratio of detected coincidences over the number of target-like nuclei. In addition, our results for the fission probability of ^{237}U induced by the ^{238}U(d,t) reaction can be compared with the results obtained in direct kinematics by Sinha et al. [Sin92] with the same reaction. Finally, **the validity of the Weisskopf-Ewing approximation can be verified** by comparing our results for the ^{238}U(d,t) reaction with the those from the ^{238}U(^{3}He,^{4}He) reaction measured by the CENBG collaboration in regular kinematics [Jur17] and with the available neutron-induced data for the n+^{236}U reaction.

The (d,p) reaction is understood as a two-step process, first the deuteron breaks up into proton and neutron and then the neutron is absorbed by the target nucleus, eventually leading to the formation of a CN. However, the neutron can escape before the formation of the (A+1)* CN, leaving the nucleus A in the ground state or in an excited state. The first case is called elastic break-up and the second inelastic breakup. This means that the detection of a proton does not necessarily imply that the (A+1)* CN has been formed. Unlike γ or neutron emission, fission can only proceed through the formation of a CN [Sch18]. Consequently, if we detect protons that are not related to the formation of the ^{239}U* CN, according to eq. (2), the measured fission probability will be underestimated with respect to its real value. ^{239}U is very similar to ^{237}U and we expect that the WE approximation is valid for ^{239}U. Thus, the real value of the fission probability induced by the (d,p) reaction will be very close to the neutron-induced fission probability. We can then evaluate the amount of the elastic or inelastic breakup by comparing our fission probability with the neutron-induced one.

A. Moro and J. Lei have performed calculations based on the Distorted Wave Born Approximation (DWBA) for the ^{238}U(d,p) reaction [Duc16]. They predict that approximately 80% of the ^{238}U(d,p) cross section leads to the formation of CN ^{239}U*. In [Duc16] the CENBG investigated the ^{238}U(d,p) reaction in direct kinematics, but it was not possible to validate the calculations due to the presence of target contaminants. This problem will be solved with **SUNRISE,** which **will provide very precious information for constraining the models describing the deuteron** elastic and inelastic **break-up.**

Reaction	Telescope angle	Telescope solid angle	Cross section	Detected events	Required beamtime
^{238}U(d,p) [Lei19]	40±0.5°	0.042 sr	130 mb/sr	0.11 Hz	0.53 days
^{238}U(d,d') [Cha19]	40±5°	0.42 sr	1 mb/sr	0.0084 Hz	6.9 days

Table 4: Values used to estimate the beam time necessary to measure the decay probabilities as a function of the excitation energy at a telescope angle of 40° with a relative uncertainty of 10%.

The luminosity after injection of the cooled beam into the CRYRING is $L_0=N_0 \cdot f \cdot N_t$, where N_0 is the number of $^{238}U^{92+}$ injected ions, f is the revolution frequency (0.85 MHz at 11 A MeV) and N_t is the effective number of deuterium target atoms, which depends on the overlap between the beam and the target. The lifetime τ of the stored $^{238}U^{92+}$ ions is determined by e^- capture reactions in the gas-jet target, the e^- cooler and the residual gas. With a beam emittance of 0.5 mm·mrad, a target of 0.5 mm radius and thickness of $4 \cdot 10^{13}$ atoms/cm^2, the lifetime of $^{238}U^{92+}$ is estimated to be τ=4 s. Therefore, the instantaneous luminosity L will clearly decrease as a function of time, $L(t)= L_0 \cdot e^{(-t/\tau)}$. To estimate the counting rates we have to consider the average luminosity during a measurement cycle of duration T:

$$\langle L \rangle = \frac{\int_0^T L_0 \cdot e^{-\frac{t}{\tau}} \cdot dt}{T} \quad (3)$$

If we assume T=40 s -which is the typical time it takes to decelerate and cool the beam at the ESR- and $N_0=2 \cdot 10^7$, then the average luminosity during one measurement cycle is **$\langle L \rangle \approx 2 \cdot 10^{25}$ cm^{-2}·s^{-1}**. To determine with our set-up the decay probabilities as a function of E^* at a given target-like angle with a relative uncertainty of about 10%, we need to detect 5000 target-like residues. Table 4 shows the beam time necessary to reach this statistics at 40° for the ^{238}U(d,p) and ^{238}U(d,d') reactions at 11 A MeV. The cross sections for the two reactions were estimated with Continuum Discretized Coupled Channels (CDCC) and DWBA calculations [Lei19, Cha19]. We see that for the ^{238}U(d,d') reaction it is necessary to sum up the events over a larger angular interval around 40° to reach the required statistics in a reasonable time. The situation can be considerably improved if 10^8 ions can be injected, which shall be possible with the optimization of the ESR deceleration capabilities in the next years.

3. Work plan

The project is structured in four work packages (WP). The duration of the tasks during the first three years of the project is given in the Gantt chart shown in Table 5.

WP1: Definition of detectors and associated electronics

***Task 1.1. Definition and purchase of detectors for Si telescopes:** We will perform simulations to conclude the definition of the geometry, segmentation, thickness and position of the ΔE and E detectors. We will contact the detector suppliers and order the detectors. This task must be performed at the beginning of the project because the production of thick Si(Li) takes typically one year, and the size and the detector properties are needed for the following tasks.

***Task 1.2. Definition and purchase of readout electronics for Si telescopes:** According to the results of Task 1.1, we will define the cables to transport the signals inside the pocket and the feedthroughs to take them outside the pocket, as well as the electronic readout and processing modules that follow.

***Task 1.3. Definition of fission detector and development of preamplifiers:** This detector is foreseen to be made of solar cells that will work as an active window of a pocket. First, the simulations to optimize the geometry and segmentation of the fission detector will be concluded. Once all the characteristics are defined, cables, feedthroughs and solar cells will be purchased. The signals of the cells will be delivered to specific designed pre-amplifiers, adapted to the large capacitance of the cells and the dynamic range of the input signals.

***Task 1.4. Definition of the heavy-residue detector and associated electronics:** We will conclude the simulations to optimize the geometry, segmentation and position of the heavy residue detector. This task will take several months as it requires a systematic study of all the reactions and target-like angles of interest to optimize the separation from the elastic-scattering residues.

WP2: Design and production of the target detector station

***Task 2.1. Technical design and purchase of the target reaction chamber:** The target reaction chamber will be coupled to the gas-jet target of the CRYRING. The complex pumping system of the

gas jet will constrain the size of the chamber. Moreover, the geometry and position of the detectors and electronics from tasks 1.1, 1.2 and 1.3 will further define the main structure of this chamber. To ensure UHV compatibility, the stainless steel of the chamber will be carefully selected and undergo a firing vacuum treatment, which reduces the amount of hydrogen trapped in the walls. A high-level pumping system will be used, including NEG coating of the chamber, useful to contain the outgassing of heavier elements.

***Task 2.2. Technical design and purchase of the manipulator for the telescopes:** At the beginning of the experiment, while the ring is being adjusted, the beam pipes of the ring should be empty to avoid accidental collisions of the direct beam with any obstacle. Therefore, the telescope pockets have to be connected to a manipulator that will set them in and out of the reaction chamber. The manipulator will be activated by a motor. The design of the pockets housing the detectors and the cables will be done according to the results of Tasks 1.1. and 1.2. Due to the very delicate UHV conditions outside the pocket, special care should be taken in the definition of the pocket material and the vacuum pumping system, as well as the welding of the stainless-steel window.

***Task 2.3. Technical design and purchase of the manipulator for the fission detector:** The principle of this manipulator is the same as the one of task 2.2, except that in this case the pocket will have large active windows made of solar cells. The pocket will house the cables in auxiliary vacuum. The design of the manipulator will be based on the outcome of task 1.3. Work is required to ensure the UHV-compatibility of the cells and the supports, and to avoid leakages.

***Task 2.4. Assembly of manipulators in the reaction chamber and general test of detector station:** Once tasks 2.1, 2.2 and 2.3 are completed, the manipulators will be coupled to the target reaction chamber without the detection systems. The pocket movement, motor control system and position precision will be tested. Afterwards, the detectors and the cables will be placed inside the pockets to test the positioning of the detectors, the movement of cables within the manipulators, the readout electronics and the vacuum system.

WP3: Design and production of the detector station for heavy residues

***Task 3.1. Design and purchase of the manipulator and the chamber for the heavy-residue detector:** This task will start with the evaluation of the space available in the CRYRING section where the focal point is located. This section will require a rearrangement of the elements already in place. This evaluation and the outcome of task 1.4 will define the constraints for the design of the chamber and the manipulator. The system is similar to the ones that already exist at CRYRING.

***Task 3.2. Assembly and general test of the heavy-residue detector station:** Once the production of the chamber and manipulator are concluded, these will be coupled and tested. Then, we will test the positioning mechanism, the detectors, the electronics and the vacuum system.

WP4: Experiment, data analysis and results

***Task 4.1. Preparation and submission of proposal to the PAC:** The next Proposal Advisory Committee (PAC) of FAIR will presumably take place in April 2020. We will prepare and submit a proposal to study surrogate reactions induced by a ^{238}U beam on a D_2 target with the set-up developed within this project.

***Task 4.2. Implementation of the target detector station into the CRYRING:** After task 2.4, we will install the target detector station in the target section of the CRYRING. The installation will also include the setup of the electronic readout chain. After installation and depending on the date of the experiment, a bake out procedure will be started.

***Task 4.3. Implementation of the heavy-residue detector station into the CRYRING:** After completion of task 3.2, both partners will install the heavy-residue station at the focal point of the CRYRING.

***Task 4.4. Setting the acquisition system and realization of experiment:** We will prepare the software for the data acquisition system before the experiment starts. After tasks 4.2 and 4.3, we will use the set-up to conduct the experiment.

***Task 4.5. Data analysis and interpretation of results:** During the last two years, the data will be analyzed and the results interpreted in collaboration with theoreticians from the CEA and the University of Sevilla.

Table 5: Gantt chart for the first three years. HR stands for Heavy Residue. Prod. for production.

WP	Task	Year 1												Year 2												Year 3											
		1	2	3	4	5	6	7	8	9	10	11	12	1	2	3	4	5	6	7	8	9	10	11	12	1	2	3	4	5	6	7	8	9	10	11	12
1	1.1- Definition telescopes																																				
	1.2- Electronics telescopes																																				
	1.3- Fission detec. & preamps																																				
	1.4- Definition HR detector																																				
2	2.1- Prod. Target Reaction Chamber																																				
	2.2-Prod. manipulator telescopes																																				
	2.3- Prod. manipulator fission detector																																				
	2.4-Assembly and tests																																				
3	3.1-Prod. chamber& manipulator HR																																				
	3.2- Assembly of HR station																																				
4	4.1- Experiment Proposal																																				
	4.2- Target station implementation																																				
	4.3-HR station implementation																																				
	4.4- Experiment and analysis																																				

4. Requested ressources

***Equipment:**
-Purchase of Si(Li) detectors and DSSSDs for telescope (tasks 1.1): 150000 €
-Purchase of cables and readout electronics for telescopes (task 1.2): 100000 €
-Within task 1.2, purchase of feedthrougs and power supply for DSSSDs & Si(Li) detectors: 50000 €
-Building fission detector and related electronics (task 1.3): 40000 €
-Purchase of Heavy Residue detector and related electronics (task 1.4):40000 €
-Production of target reaction chamber (task 2.1): 70000 €
-Building manipulators for telescopes and fission detector (tasks 2.2 and 2.3), including bellows, pockets, control systems, flanges, detector supports: 150000 €
-Vacuum system for target chamber and manipulators for telescopes and fission detector (tasks 2.1, 2.2, 2.3). NEG coating of the target chamber. We need primary, turbo and adsorption pumps, valves, gauges, heating jackets, heating bands and gaskets: 120000 €
-Building station for heavy-residue detector (task 3.1), including pocket, manipulator, motor, control and vacuum systems: 80000 €
-Two additional pockets with beam monitors to verify the position of the beam on the target are needed: 200000 €
***Personnel:** 1 PhD student for the three last years, for mounting the set-up, participating to the measurement, data analysis and interpretation of results in collaboration with theoreticians.
***Travel:**
-We benefit from the CNRS-GSI agreement number 19-80 that covers part of the stay of French researchers at GSI and of German researchers in France. Still, we need financial support to cover the trips of researchers and engineers of the CENBG to travel to Germany for collaboration meetings and experiments: 10000 €/year except for the year of the experiment (presumably 2023) for which we request 20000 €.

5. Impact and benefits of the project

SUNRISE will set the basis for a **new generation of high-resolution measurements of decay probabilities in inverse kinematics**. This type of measurements can be also conducted at **other facilities** like the future heavy-ion ring of HIE-ISOLDE, the CSRe or the Rare-RI ring. The radioactive beams produced in these facilities are highly complementary to those of GSI/FAIR. Hence, we will be able to conduct systematic measurements of the decay probabilities for all open decay channels of a huge number of nuclei. Our project will thus be **a major component** of the coordinated nuclear physics efforts **to improve our understanding of the conditions of the s-process environments and to find a solution of the longstanding mystery of the r-process astrophysical sites.** Apart from the indirect determination of neutron cross sections, the data measured with the technology developed in SUNRISE will allow us to study fundamental properties of nuclei like fission barriers, particle transmission coefficients, γ-ray strength functions and level densities. Their evolution over long isotopic chains will provide the foundation for a **better understanding of the nucleon-nucleon interaction**.

The technical developments carried out will be very **beneficial for many other in-ring experiments**. For example, the new detector station at the focal point will enable the complete separation of the proton-capture residues from the elastic scattered residues, which represent one of the major backgrounds in the measurement of proton-capture cross sections [Mei15, Glo19]. This station will also be of great advantage for atomic-physics experiments aiming at the measurement of e^--capture cross sections on heavy nuclei, since at the focal point there is a very clean separation of the e^--capture residues from the unreacted beam. The development of the particle telescope will be very useful for normalizing the proton-capture cross sections with proton elastic cross sections in cases when the produced x-rays cannot be detected. Nuclear-structure experiments to study the

properties of low-lying states of exotic nuclei via inelastic scattering and transfer reactions will also profit from our telescope.

This project will also be the **seed of a unique program of fission studies**. If the fission detector shows the expected performances in terms of time and energy resolution, and with the appropriate segmentation, it will also be possible to measure the velocities and the kinetic energies of both fission fragments. In fact, because of the very small energy loss and straggling of the fragments in the ultra-thin gas-jet target and the absence of matter between the target and the fission detector, storage rings are particularly well suited for the measurement of the velocity and kinetic energy of the fragments. Interestingly, with these two quantities it is possible to determine the fragment masses before and after prompt neutron emission [Mul84]. Therefore, in addition to the fission probability, we would be able to directly measure the fission-fragment kinetic energies and mass yields as a function of excitation energy.

Our detector and methodology studies are also of interest for the realization of a **long-term, very ambitious facility to directly measure neutron-induced cross sections in inverse kinematics**. The idea is to build a neutron target by coupling a storage ring with a strong neutron source (e.g. reactor or spallation source). More precisely, one of the beam pipes of the storage ring goes through or close by the neutron source. The produced neutrons can easily penetrate the beam pipe creating a kind of neutron gas, which constitutes the neutron target. Neutron densities of about $10^9/cm^2$ can be obtained with a spallation source [Rei17]. The key idea of this project is that the revolution frequency of the stored beam leads to a significant increase of the effective neutron-target thickness, which allows measurements of neutron-induced cross sections in inverse kinematics for beams with half-lives as low as few minutes. The measurement of neutron-induced fission cross sections with a reasonable efficiency at this facility is only possible for beam energies above about 10 AMeV. Therefore, our project is complementary to this future facility, as it can give indirect access to neutron cross-sections for nuclei with lower half-lives, down to few seconds, and to (n,f) cross sections below 10 MeV neutron energy.

The present project has the potential to lead to interesting industrial spin-offs. Apart from the interest for beam diagnostic, the developments undertaken to use solar cells as detectors for energetic heavy ions can be of interest for space research. Spacecrafts operating in the inner Solar System usually rely on solar panels to derive electricity from sunlight. Spacecrafts are subject to an intense flux of cosmic rays consisting of high-energetic charged particles ranging from protons to iron and even beyond. One could envisage using the solar panels to detect these nuclei.

6. Collaboration

CENBG: B. Jurado (Coordinator), A. Henriques (Marie Curie post-doc), PhD Student, J. Pibernat, B. Thomas, L. Mathieu, I. Tsekhanovich, P. Alfaurt.
IPNO: L. Audouin
CEA-Bruyeres le Chatel: L. Gaudefroy, V. Meot, O. Roig, M. Dupuis, J. Taieb, A. Chatillon
CEA-Cadarache : O. Bouland
GSI/FAIR: J. Glorius, Y. Litvinov, M. Lestinsky
Max-Planck Institute for Nuclear Physics Heidelberg: M. Grieser
University of Frankfurt: R. Reifarth, Ch. Langer

References

[Aji91] N.N. Ajitanand et al., Nucl. Instr. Meth. A 300 (1991) 354
[Bou12] G. Boutoux, B. Jurado et al., Phys. Lett. B 712 (2012) 319
[Bur57] E. M. Burbidge et al., Rev. Mod. Phys. 29 (1957) 547
[Canbe] https://www.mirion.com/
[Cha19] P. Chau, private communication 2019
[Duc16] Q. Ducasse, B. jurado et al., Phys. Rev. C 94 (2016) 024614

[Eic15] M. Eichler et al., Astrophys Journal, 808:30 (2015)
[Esc12] J. E. Escher et al., Rev. Mod. Phys. 84 (2012) 353
[Esc18] J. E. Escher et al., Phys. Rev. Lett. 121, 052501 (2018)
[Fra87] B. Franzke, Nucl. Instr. Meth. B 24 (25) (1987) 18
[Gau97] C. Gautherin, PhD Thesis , CEA-SAclay, 1997
[Glo19] J. Glorius et al., Phys Rev Lett 122 (2019) 092701
[Gor15] S. Goriely, Eur. Phys. J. A (2015) 51: 22
[Gri19] M. Grieser, private communication 2019 ; M. Grieser et al., Eur. Phys. J. Special Topics 207 (2012) 1
[Hef15]T. Heftrich et al., Phys. Rev. C 92 (2015) 15806
[Hsi81] C. Hsieh et al., Electron Device Letters,IEEE 2 (1981) 103
[Jur17] B. Jurado et al., EPJ Web of Conferences 146 (2017) 11006
[Kas17] D. Kasen, et al., Nature 551 (2017) 80
[Kes10] G. Kessedjian, B. Jurado, et al., Phys Lett. B 692 (2010) 297
[Kes15] G. Kessedjian, B. Jurado, et al. Phys. Rev. C 91 (2015) 044607
[Lan14] C. Langer et al., Phys. Rev. C 89 (2014) 35806
[Lei19] J. Lei and A. Moro, private communication 2019
[Les16] M. Lestinsky et al., Eur. Phys. J. Special Topics 225 (2016) 797–882
[Mei15] B. Mei et al., Phys. Rev. C 92 (2015) 035803
[Micro] www.micronsemiconductor.co.uk/
[Mul84]R. Müller et al., Phys. Rev. C 29 (1984) 885
[Nucar] Nuclear Astrophysics at storage Rings: http://exp-astro.physik.uni-frankfurt.de/nucar/
[Per19a] R. Perez, PhD Thesis, University of Bordeaux, 2019
[Per19b] R. Perez, B. Jurado et al., accepted Nucl. Inst. Meth., https://arxiv.org/abs/1901.04874
[Pet04] M. Petit et al., Nucl. Phys. A 735 (2004) 345
[Pig10] M. Pignatari, The Astrophysical Journal 710 (2010) 1557
[Pig16] M. Pignatari, K. Goebel, R. Reifarth, et al., Int. J. Mod. Phys. E 25 (2016) 1630003
[Rat19] A. Ratkiewicz et al., Phys. Rev. Lett 122 (2019) 052502
[Rei14] R. Reifarth et al., J. Phys. G: Nucl. Part. Phys. 41 (2014) 053101
[Rei17] R. Reifarth et al., Phys. Rev. Accel. Beams 20 (2017) 044701
[Rei18]R. Reifarth et al, Eur. Phys. J. Plus 133, 424 (2018)
[Sch16] K.-H. Schmidt, B. Jurado et al., Nucl. Data Sheets 131 (2016) 107
[Sch18] K.-H. Schmidt and B. Jurado, Rep. Prog. Phys. 81 (2018) 106301 (64pp)
[Sci10] N. D. Scielzo et al., Phys. Rev. C 81 (2010) 034608
[Sie79] G. Siegert, Nucl. Instr. Meth. 164 (1979) 437
[Sin92] A. K. Sinha et al., J. Phys. G: Nucl. Part. Phys. 18 (1992) L105
[Str11] B. Streicher et al., Nucl. Instrum. Meth. A 654 (2011) 604
[Thi17] F.-K. Thielemann et al, Annual Review of Nuclear and Particle Science 64 (2017) 253
[Wei17] M. Weigand, et al., Phys. Rev. C 95 (2017) 15808
[Xia02] J.W. Xia et al., Nucl. Instr. Meth. A 488 (2002) 11
[Yam13] Y. Yamaguchi et al., Nucl. Instr. Meth. B (2013) 629